



**20th IAEA Fusion Energy Conference
Vilamoura, Portugal, 1 to 6 November 2004**

IAEA-CN-116/EX/6-4Rb

**PLASMA ROTATION IN ELECTRON CYCLOTRON
HEATED H-MODES IN DIII-D**

J.S. deGrassie, K.H. Burrell, L.R. Baylor 1), W.A. Houlberg 1), W.M. Solomon 2)

General Atomics
San Diego, California 92186-5608
United States of America

-
- 1) Oak Ridge National Laboratory, Oak Ridge, Tennessee 37381, USA
2) Princeton Plasma Physics Laboratory, Princeton, New Jersey, USA

This is a preprint of a paper intended for presentation at a scientific meeting. Because of the provisional nature of its content and since changes of substance or detail may have to be made before publication, the preprint is made available on the understanding that it will not be cited in the literature or in any way be reproduced in its present form. The views expressed and the statements made remain the responsibility of the named author(s); the views do not necessarily reflect those of the government of the designating Member State(s) or of the designating organization(s). In particular, neither the IAEA nor any other organization or body sponsoring this meeting can be held responsible for any material reproduced in this preprint.

Plasma Rotation in Electron Cyclotron Heated H-modes in DIII-D

J.S. deGrassie 1), K.H. Burrell 1), L.R. Baylor 2), W.A. Houlberg 2), W.M. Solomon 3)

1) General Atomics, P.O. Box 85608, San Diego, California, 92186-5608, USA

2) Oak Ridge National Laboratory, Oak Ridge, Tennessee 37381, USA

3) Princeton Plasma Physics Laboratory, Princeton, New Jersey, USA

email: degrassie@fusion.gat.com

Abstract. Toroidal rotation profiles of C^{+6} in DIII-D electron cyclotron heated (ECH) H-modes are hollow, with co-rotation (parallel to I_p) in the outer region and reduced, or counter-rotation in the core. This is in contrast to relatively flat profiles in ohmically heated (OH) H-modes. The auxiliary injected toroidal torque in these discharges is negligible. The rotation profile is mildly sensitive to the details of the ECH power deposition profile only in the very center of the plasma. The outer region co-rotation peak is found to scale with $(W/I_p)(\bar{T}_{e0}/\bar{T}_{i0})$, across all ECH deposition profiles, OH H-mode or L-mode. Here W is the stored thermal energy, and \bar{T}_{e0} and \bar{T}_{i0} are core averaged electron and ion temperatures. The rotation velocity measured at the outboard last closed flux surface is not zero. The measured boundary value is commensurate with simple estimates of an averaged parallel velocity for a loss cone ion velocity distribution. Most DIII-D ECH H-mode data are from ELM-free periods, in which the kinetic and rotation profiles are evolving. In helium ECH H-modes, the rotation profiles for He^{+2} and C^{+6} are hollow. The helium discharges have ELMs and demonstrate that the ELM-free state is not necessary for counter core rotation.

1. Introduction

In the tokamak, the flow velocity, V , and its shear are important for issues of stability [1] and confinement [2]. Tokamak discharges invariably have nonzero toroidal velocity, V_ϕ , and hence toroidal mechanical angular momentum. Large toroidal rotation velocities are driven by the auxiliary injected torque from directed neutral beam injection (NBI) [3]. The relatively smaller rotation velocity driven by radio frequency (RF) heating with waves carrying toroidal momentum has been verified experimentally [4]. There is a growing body of experimental data on toroidal rotation in the absence of any auxiliary injected torque [5–7], typically with magnitudes smaller than observed with NBI. Ultimately a burning plasma will not have NBI, at least not into the interior, and thus it is important to understand this ‘non-driven’ rotation. Even with RF momentum injection, the driven level is in addition to some comparable ambient non-driven background rotation [4].

In DIII-D, experiments have been done to measure the rotation profiles in H-modes generated with electron cyclotron heating (ECH) [7]. As a natural comparison, we also measure profiles in H-modes arising from Ohmic heating (OH) only. Even with electron cyclotron current drive (ECCD) the toroidal photon momentum is negligible; so these discharges are without auxiliary torque, or non-driven, as we shall refer to such cases. The edge of an axisymmetric discharge of course can exchange momentum with the boundary [8], but we do not include this in our definition of a driving torque.

In recent years, a number of experiments have been reported from the C-Mod group on non-driven rotation [5,9]. The reader is referred to the references for the details and subtleties. For this paper, we summarize some key points from C-Mod experiments. OH H-modes and RF H-modes with enhanced recycling (EDA H-mode) have a flat V_ϕ profile in minor radius, with V_ϕ in the co-rotation direction. In contrast, ELM-free RF H-modes have a velocity profile peaked on axis. These cases are modeled with a momentum diffusivity χ_ϕ , a momentum pinch velocity, v_{pr}/a , where r/a is the normalized minor radius, and a boundary value of $V_{\phi 1}$. These three parameters are fit to the measured temporally developing V_ϕ profile. In EDA H-modes χ_ϕ is found to be small compared to χ_{eff} , the total thermal diffusivity, and no pinch is necessary. The flat profile evolves from the boundary condition.

In the ELM-free case χ_ϕ is comparable to χ_{eff} and a nonzero inward v_p of 10 m/s is found necessary to produce the peaked profile. Off-axis resonant RF heating in C-Mod can result in an EDA H-mode temporally developing an internal transport barrier (ITB) with the rotation in the interior reversing to the counter direction. The above model is not forced to describe this reversal nor is it clear that it should.

The toroidal rotation profiles measured in DIII-D ECH H-modes are clearly different from those in OH H-modes, which are relatively flat, as in C-Mod. There is a greater shear in the rotation profile, with V_ϕ in the co-direction in the outer region and depressed, or even in the counter-direction, in the core region. In this paper we will describe the measurement technique and the characteristics of the measured rotation profiles with varying ECH deposition profile. Three deposition profiles are utilized, labeled as ‘core’, ‘spread’, and ‘off-axis’, and described in Section 3. The measured boundary velocity, $V_{\phi 1}$, is indeed nonzero and is described in Section 4. The temporal evolution described in Section 5 shows that the counter rotation in the core develops in time after the ECH H-mode transition and then dies away with rising density in an ELM-free regime. Lastly we describe the hollow rotation profile for the bulk ion, He^{+2} , in a helium ECH H-mode discharge.

2. Measurement Technique

The details of the ion V , and temperature, T_i , measurements in these experiments have been presented [7]. Briefly, charge exchange recombination (CER) spectroscopy [10] is used. In the majority of these experiments we measure the velocity of C^{+6} , an intrinsic impurity. In selective cases neoclassical theory (NC) [11] is used to compute the main ion, D^+ , velocity. The CER technique requires NBI and the beam toroidal torque is such that only 2–4 ms of

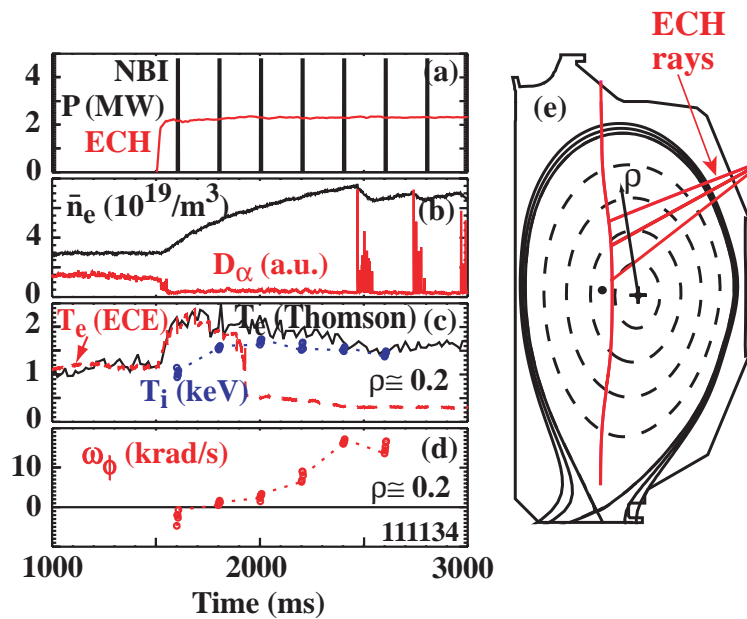


FIG. 1. ECH H-mode, $I_p = 1.3$ MA, $q_{95} = 3.5$. (a) ECH and NBI power (b) \bar{n}_e and D_α (c) core T_e , T_i (during NBI) at $\rho \sim 0.2$. T_e (ece) is cut-off $t > 2000$ ms. (d) ω_ϕ (core) builds up with each co NBI blip until ELMs commence. (e) ECH rays for ‘spread’ type of launch, from four outboard gyrotrons, using vacuum ray tracing. Power from two gyrotrons is launched along the middle ray. Vertical line indicates the second harmonic absorbing resonance for $f_{EC} = 110$ GHz.

NBI can be used before the rotation state is altered [7]. The driven rotation from a blip lingers to the extent that typically only one unperturbed measurement is made in a shot. This means that we do not have continuous temporal records as in C-Mod, where emission from a partially stripped higher Z impurity is measured passively. Temporal profile evolution is built up on a shot-to-shot basis with care to monitor other discharge characteristics in order to verify a close match. We have also measured both the main ion and C^{+6} velocities using CER in helium discharges, finding the same hollow rotation profile signature in ECH H-modes for both species.

The time history of a typical ECH H-mode discharge is shown in Fig. 1. The H-mode transition takes place less than

25 ms after the initiation of ECH power of just over 2 MW. The deposition location in the lower single-null discharge is indicated in Fig. 1(e). With ECH deposition into the central region, $\rho < 0.5$, these discharges have a long ELM-free period as indicated by the recycling D_α time trace and the rise in line averaged electron density, \bar{n}_e . Here, ρ is the normalized toroidal flux minor radius coordinate. The near-central ($\rho \sim 0.2$) electron and ion temperatures, T_e and T_i , are shown in Fig. 1(c). By $t = 2400$ ms in this discharge, the density rise cuts off all of the ECH power from being deposited at the nominal locations shown in Fig. 1(e), determined from computations with the ray tracing code TORAY_GA [12]. A train of 10 ms NBI blips is injected as shown. Two DIII-D D beam sources [13] are used, delivering 2.5 and 2.8 MW, respectively. The total beam torque is approximately 1 Nt-m/MW. The number of gyrotrons utilized varies to some extent between discharges due to trips of one or more systems, or the number of gyrotrons available on the day of an experiment. Typically each gyrotron delivers $\cong 0.5$ MW of total electron heating to the plasma. Beyond this variability no dedicated ECH power scaling experiment has been performed as yet.

The time of this first blip is moved from shot to shot for a time sequence. The subsequent blips are used to investigate beam driven momentum build up in the discharge. The core rotation frequency, $\omega_\phi = V_\phi/R$, measured at each blip is shown in Fig. 1(d), where R is the major radial location. The rotation builds up with each blip until the onset of ELMs. Analysis with TRANSP [14] shows that the discharge is essentially storing all of the NBI torque during this rise. This effect precludes obtaining more than one unperturbed measurement in a discharge when coupled with the 2 s pulse limit on some DIII-D gyrotrons. When using spline fits to profiles for data manipulation we consider ω_ϕ to be a flux function.

3. Rotation Profiles

The toroidal rotation profiles show distinct signatures depending upon the type of discharge, a distinction which includes the ECH deposition location. Although many of the profiles are measured while the discharge parameters are evolving, grouping them by heating type nevertheless brings out these signatures, and establishes the common features beyond showing individual examples. The presently analyzed data set from DIII-D is summarized in Fig. (2) where we plot the simple mean values of rotation frequency sorted by discharge type, versus ρ . For this data set, the toroidal magnetic field is $B_{T0} = 1.75$ T, and the range of plasma current, I_p , is 1–1.5 MA. The averages are taken over the set of first time slices from discharges of one type. These may have differing delays after the H-mode transition, or different values of I_p or X-point height, density, temperature, and possibly ECH power. The

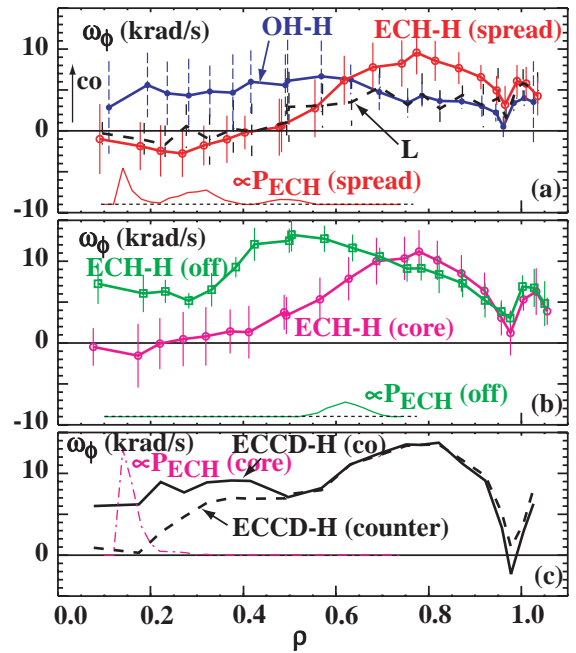


FIG. 2. Set-averaged rotation profiles, with m discharges in a set (a) ‘L-mode’ (dash, $m=5$), OH-H (\bullet , $m=6$), spread-ECH-H (\circ , $m=16$), (b) core-ECH-H (\circ , $m=12$), off-axis ECH-H (\square , $m=5$), (c) single discharge co- and counter-ECCD-H with core deposition. EC power deposition profiles are indicated. The core deposition profile for (b) is indicated in (c). The error bars are the standard deviations for the discharges in the set and exceed the intrinsic measurement error.

error bars indicated show the standard deviation over a set, due to this variability of the plasma conditions. These deviations typically dominate over the intrinsic measurement error. The ECH deposition profile is indicated for types with EC power. In spite of including non-identical discharges within a type, the rotation profile signatures clearly emerge.

All ECH H-mode rotation profiles are hollow. The L-mode time slices (pre H-mode transition) are also hollow. Only the OH H-mode profiles are flat. A feature common to all is the co-rotation for $\rho \sim 0.6-0.9$. This co-rotation is greater for the ECH H-modes, correlated with greater plasma stored thermal energy, W , as described below. The central rotation, $\rho < 0.3$, varies with ECH deposition. The most reversed (counter-directed) core rotation is observed in some discharges with the ‘spread’ deposition profile shown in Fig. 2(a). ‘Core’ deposition results in a similar profile [Fig. 2(b,c)] while the ‘off-axis’ deposition gives a clearly different profile, hollow but non-reversed in the core [Fig. 2(b)]. Additionally two individual profiles are shown in Fig. 2(c) for two discharges with ECCD in core deposition, one co- and one counter-ECCD, respectively. These are nearly identical for $\rho > 0.5$ and diverge from one another as the magnetic axis is approached. Presently, the ECCD data set is limited. These ECCD H-modes have a large T_e/T_i in the core, relative to the rest of this dataset. Although the rotation profiles do show some change with ECH deposition location, especially for ‘off-axis’ deposition, we have not yet found a compelling detailed correlation between rotation, or its gradient, and the kinetic profiles or their gradients.

The amplitude of the peak in V_ϕ near $\rho \sim 0.8$ increases with W/I_p . This scaling has been reported for core incremental co-velocities in C-Mod for OH and RF H-modes [9]. For the DIII-D data set, this is shown in Fig. 3(a) where we plot $V_{pk} = V_\phi$ averaged over three CER channels at $0.74 < \rho < 0.81$, versus W/I_p . The line is a simple best fit and serves to separate different H-mode types. The larger V_{pk} values are from discharges with core deposition resulting in greater central T_e/T_i . Accordingly, we find a much better correlation in Fig. 3(b) plotting V_{pk} versus $(W/I_p)(\bar{T}_{e0}/\bar{T}_{i0})$, where \bar{T}_{e0} is averaged over several Thomson scattering channels for $\rho < 0.25$ and similarly for the CER-measured ion temperature. In Fig. 3(c) we show the lack of correlation between $\bar{T}_{e0}/\bar{T}_{i0}$ and W/I_p , that is, these are effectively independent parameters for this data set. Using a local T_e/T_i determined around $\rho = 0.8$ does not result in a similar collapse of the data points seen in Fig. 3(b) because this temperature ratio shows much less variation than in the core. No clear correlation for an averaged central V_ϕ has yet been found. Previously, we compared core co-rotation values for an OH H-mode in DIII-D with the C-Mod scaling and found similarity providing allowance is made for a size scaling [7].

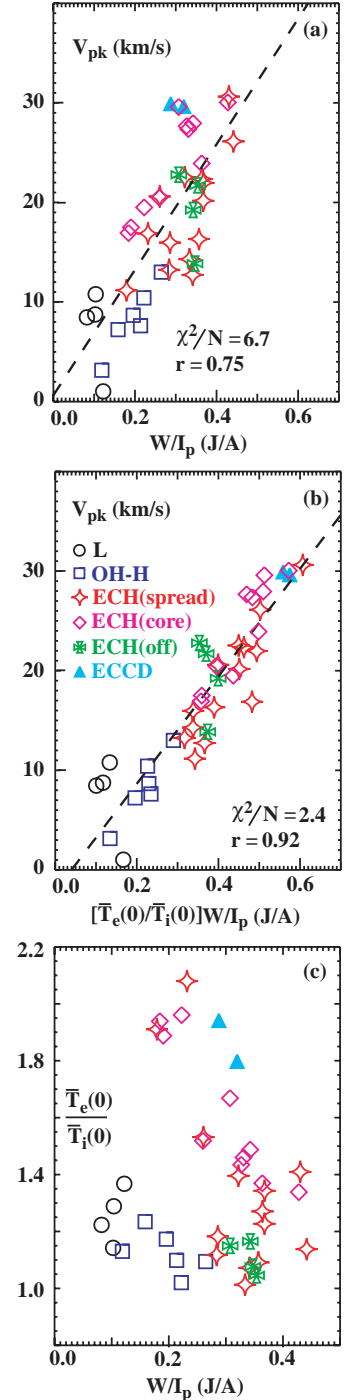


FIG. 3. (a) V_{pk} scaling with W/I_p (b) with $(W/I_p)(T_{e0}/T_{i0})$, (c) lack of correlation between $(\bar{T}_{e0}/\bar{T}_{i0})$ and W/I_p . V_{pk} is V_ϕ averaged over $0.74 < \rho < 0.81$. r is the correlation coefficient.

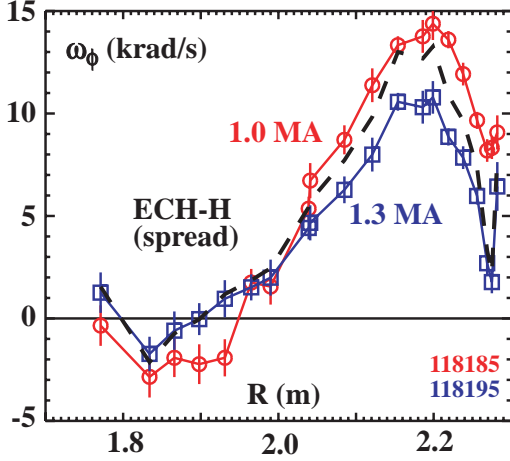


FIG. 4. Rotation profiles for ECH H-modes, high (\square) and low (\circ) I_p , and high case scaled to the low as indicated by Fig. 3(b) (dashed line).

The variability giving rise to the deviations seen in the averaged profiles shown in Fig. 2 is much less when systematic changes are made to one type of discharge. For example, profiles for two discharges with different I_p are shown in Fig. 4. The lower I_p discharge has the greater V_{pk} , in keeping with Fig. 3(b). The dashed line in Fig. 4 shows the higher I_p profile scaled by the ratio of $(W/I_p)(\bar{T}_{e0}/\bar{T}_{i0})$ for the two discharges and there is agreement in the scaled V_{pk} values, but there is no strong evidence of scaling for the core velocities, other than that the velocities are small here. The shape for the 1.0 MA discharge is similar to Fig. 1(d), but the X-point is higher above the vessel floor for the 1.3 MA in order to stay away from the OH H-mode threshold.

4. Boundary Value

Theoretical models addressing non-driven toroidal rotation require a boundary value, $\omega_{\phi 1} = V_{\phi 1}/R_1$, in order to make absolute predictions for rotation profiles [15–18]. Typically $\omega_{\phi 1}$ is assumed to be 0, given the lack of experimental data. (Here R_1 is the boundary surface major radius at the CER viewing height.) In DIII-D we have measurements of $\omega_{\phi 1}$ for this data set, using viewing channels at or very close to R_1 . As seen in Fig. 2, $\omega_{\phi 1}$ is nonzero for the averages over the sets, with relatively small deviations. The simple overall averaged value for this set is $\omega_{\phi 1} = 4.8 \pm 1.6$ krad/s in the co-direction. However, this value needs closer scrutiny by individual discharge because there can be significant structure in ω_{ϕ} near $\rho = 1$, so that the measured $\omega_{\phi 1}$ is sensitive to the details of the equilibrium reconstruction; variations of 0.5 cm matter. The typically observed sharp local minimum in ω_{ϕ} near the edge is at the location of the H-mode electric well [19]. A dedicated experiment needs to be done wherein the edge location is varied slightly shot to shot, with all edge diagnostics brought to bear.

The ion collisionality should be considered in order to evaluate the meaning of any measured boundary rotation for C^{+6} . Namely, does it represent a fluid value or does it result from a substantially non-isotropic velocity distribution arising from a loss cone in velocity space? A collisionless loss cone would result because ions with co-velocity starting at R_1 are confined while all but deeply trapped counter-velocity orbits are not. However, C^{+6} is in the collisional regime. Carbon is the dominant impurity in these discharges, and self collisions dominate the C^{+6} collisionality. We show the collisionality profiles, and other kinetic profiles for a discharge of the spread-ECH type, in Fig. 5. Smooth spline fits to the experimental profiles are shown. Here, $v^* = R_0 q / \tau_i \bar{v} \epsilon^{3/2}$, where $\epsilon = r/R_0$, $\bar{v} = (T_i/M_i)^{1/2}$, and τ_i is the ion collision time, and $\hat{v} = \epsilon^{3/2} v^*$. This discharge has a higher C^{+6} concentration than one previously analyzed [7] and is not necessarily a representative of the data set as a whole. But the result that $v_C^* > 1$ for the H-mode data set is valid.

Any anisotropy in C^{+6} velocity near the edge should be small because of the large v_C^* there. However, there could be a loss cone in the D^+ velocity distribution at the edge, driving the co-rotation measured as $\omega_{\phi 1}$. Averaging over a Maxwellian with $T_i = 250$ eV and the loss cone from orbit computations for this shot gives an average toroidal rotation for D^+ of $\langle V_{\phi D} \rangle / R_1 = 10$ krad/s. But a careful simulation needs to be done to ascertain the resultant $\langle V_{\phi D} \rangle$, and self-consistent $\langle V_{\phi C} \rangle$, including the affect of an edge radial electric field [8]. Also,

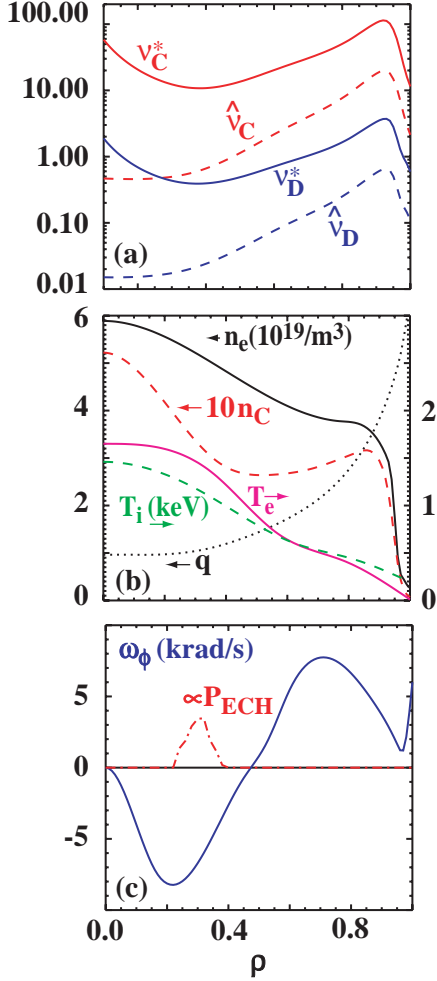


FIG. 5. Profiles for an ECH H-mode derived from smooth spline fits: (a) collisionalities v^* and \hat{v} (defined in text) for C^{+6} and D^+ . (b) n_e , n_C ($\times 10$), T_e , T_i , and safety factor, q . (c) ω_ϕ and ECH deposition.

time are shown in Fig. 6(a). An average $\bar{\omega}_\phi$ is computed for the four innermost CER channels and shown in Fig. 6(b). After the transition $\bar{\omega}_\phi$ reverses to the counter direction, becoming

the extent to which $\omega_{\phi 1}$ is a flux function might also be determined computationally. Note that this discharge is unique in that although the H-mode was initiated at $t = 1500$ ms with four gyrotrons, with deposition as in Fig. 3(a), three dropped out after ~ 50 ms and H-mode was sustained with one gyrotron, with deposition as indicated in Fig. 5(c). The discharge was ELM-free at the time of this measurement.

5. Temporal Evolution

The temporal development of toroidal rotation, ω_ϕ , in DIII-D OH H-modes is qualitatively in keeping with an edge co-momentum source diffusing inward, as modeled for C-Mod [6], although we have not yet performed a similar analysis. The L-mode state has a hollow ω_ϕ profile, as seen in the data set average in Fig. 2(a), with less co-rotation at $\rho \sim 0.8$ than in the ECH H-mode discharges. The OH H-mode rotation evolves from this to a relatively flat profile [7]. The OH H-mode set-averaged rotation shown in Fig. 2(a) is less constant since some measurement times are before the profile has come to a relatively steady condition.

In contrast, most of the DIII-D ECH H-modes to date are ELM-free during the times without significant refraction or cut-off of ECH heating rays. The resultant ω_ϕ profiles are more strongly reversed, or hollow, than the L-mode phase, and may have counter core rotation. The core ω_ϕ evolution is shown in Fig. 6 for a series of like discharges with spread heating deposition. The density and D_α evolution for the shot with the latest measurement

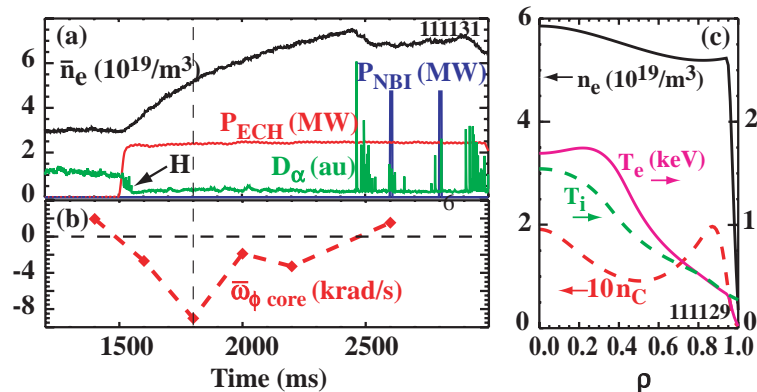


FIG. 6. (a) ECH H-mode with long ELM-free period. (b) Evolution of core rotation measured from a series of like discharges by changing the first blip time. (c) Profiles for $t = 1800$ ms from spline fits, as in Fig. 5(b).

more negative and then subsiding, eventually returning to a value near the initial one, after the onset of ELMing and the cut-off of the ECH power deposition to the core [7]. There is not a clear signature of an ITB, as is correlated with central velocity reversal in C-Mod, either in electron or ion transport in these ELM-free ECH H-modes, although careful transport analyses will be required to rule one out. The fitted kinetic profiles for the shot with the greatest negative $\bar{\omega}_\phi$, at $t = 1800$ ms, are shown in Fig. 6(c). This is a similar condition to that shown in Fig. 5, although the electron density profile, n_e , has comparatively little peaking and the carbon density, n_c , is much less. Here, $I_p = 1.1$ MA, while it is 1.3 MA for Fig. 5. (These two discharges were taken two years apart.) The T_e and T_i profiles are similar. Both have large core rotation reversal relative to this data set in spite of the differences in n_e and n_c .

The reversal to counter ω_ϕ in the core contradicts the model of a diffusive inward flow of momentum, slowly taking over the initial L-mode profile, but that has not yet penetrated the elevated T_e center on the time scale of the measurement. Adding a nonzero local v_p may model the rise in co-directed ω_ϕ between $\rho \sim 0.95$ and 0.8 (V_{pk}), but it does not provide a satisfactory model for the core reversal [6]. Additionally, a model invoking a local enhanced viscosity due to ECH [20] will not generate reversal in ω_ϕ .

It has been shown theoretically that for discharges with ICRH, even with no auxiliary momentum input, local rotation can develop due to the radially driven currents of the resonant ions coupled with momentum diffusivity [15–17], where the overall torque on the bulk plasma integrates to zero. Perhaps the key part of a similar physical mechanism is present in the core of ECH H-modes. Radial current can in principle be due to energetic electrons, although this is usually neglected due to the relatively small classical orbital excursion compared with the ion orbits. Another possible mechanism involves particle transport. A non-ambipolar net current among the total bulk, impurity and electron species has been proposed to generate the C-Mod ITB rotation reversal [18]. In the DIII-D ECH H-modes, core rotation thus driven by some localized radial current must match to the outer region, $\rho > 0.5$, which is coupled to a boundary momentum source at the wall. The boundary source penetrates by a radial pinch and diffusion. Indeed, it is possible qualitatively to generate hollow, centrally reversed, rotation profiles like those measured by applying the model in Ref. 17, Eqs. (8) and (9). For example, most simply, a local near-central counter-torque is balanced by an offsetting co-torque at larger radii with a constant diffusivity and constant inward v_p , and the boundary rotation value is matched to nonzero $\omega_{\phi 1}$.

6. ECH H-mode in Helium Discharges

Discharges with helium as the bulk ion have been utilized in order to measure the rotation profiles of both He^{+2} and C^{+6} using CER. Here, the D^+ density is $< 9\%$ of the electron density, based upon neutron production during the NBI blips. A pair of identical ECH H-mode discharges is used to get both profiles, with the spectrometers set to the appropriate emission line for each. The measured bulk He^{+2} rotation profile is also hollow, as shown in Fig. 7(a), with a large counter rotation in the core. Also shown are the measured C^{+6} profile and a neoclassical computation of the He^{+2} profile [11], based on the measured C^{+6} profile and the kinetic profiles. The neoclassical computation assumes He and C as the only ion species, with $Z_{\text{eff}} \sim 2.4$. The density and temperature profiles are shown in Fig. 7(b). These discharges have core ECH deposition, Fig. 2(c), and were ELMing during the measurement. Here, $I_p = 1.7$ MA, $q_{95} = 2.7$, a lower value to obtain ELM characteristics closer to those of the off-axis D^+ ECH H-modes. The value of V_{pk} for C^{+6} (11 km/s) falls near the fit line in Fig. 3(b). Further analysis will be done regarding the difference in the neoclassical prediction and the measured He^{+2} rotation profile. Such neoclassical computations have been verified in NBI-driven discharges using multiple impurity species in the same discharge [21].

Acknowledgment

Work supported by U.S. Department of Energy under Cooperative Agreement DE-FC02-04ER54698, and Contract Nos. DE-AC05-00OR22725, DE-AC02-76CH03073.

References

- [1] GAROFALO, A.M., et al., Nucl. Fusion **41** (2001) 1171.
- [2] BURRELL, K.H., Phys. Plasmas **4** (1997) 1499.
- [3] deGRASSIE, J.S., et al., Nucl. Fusion **43** (2003) 142.
- [4] ERIKSSON, L.-G., et al., Phys. Rev. Lett. **92** (2004) 235001.
- [5] RICE, J.E., et al., Phys. Plasmas **11** (2004) 2427, and references therein.
- [6] RICE, J.E., et al., Nucl. Fusion **44** (2004) 379.
- [7] deGRASSIE, J.S., et al., Phys. Plasmas **11** (2004) 4323.
- [8] CHANG, C.S., et al., Phys Plasmas **11** (2004) 2649.
- [9] HUTCHINSON, I.H., et al., Phys. Rev. Lett. **84** (2000) 3330.
- [10] BURRELL, K.H., et al., Rev. Sci. Instrum. **72** (2001) 1028.
- [11] HOULBERG, W.A., et al., Phys. Plasmas **4** (1997) 3230.
- [12] MATSUDA, K., IEEE Trans. Plasma Sci. **17** (1989) 6.
- [13] LUXON, J.L., Nucl. Fusion **42** (2002) 614.
- [14] ONGENA, J., et al., Trans. Fusion Technol. **33** (1998) 181.
- [15] PERKINS, F.W., et al., Phys. Plasmas **8** (2001) 2181.
- [16] CHAN, V.S., et al., Phys. Plasmas **9** (2002) 501.
- [17] ERIKSSON, L.-G, PORCELLI, F., Nucl. Fusion **42** (2002) 959.
- [18] ROGISTER, A.L., et al., Nucl. Fusion **42** (2002) 1144.
- [19] GROEBNER, R.J., Phys. Fluids B **5** (1993) 2343.
- [20] deGRASSIE, J.S, et al., "Toroidal rotation and core ion confinement with RF heating in DIII-D" Controlled Fusion and Plasma Phys. (Proc. Conf., Maastricht, 1999) Vol. 23J, European Physical Society, Nieuwegein (1999) 1189.
- [21] BAYLOR, L.R., et al., Phys. Plasmas **11** (2004) 3100.

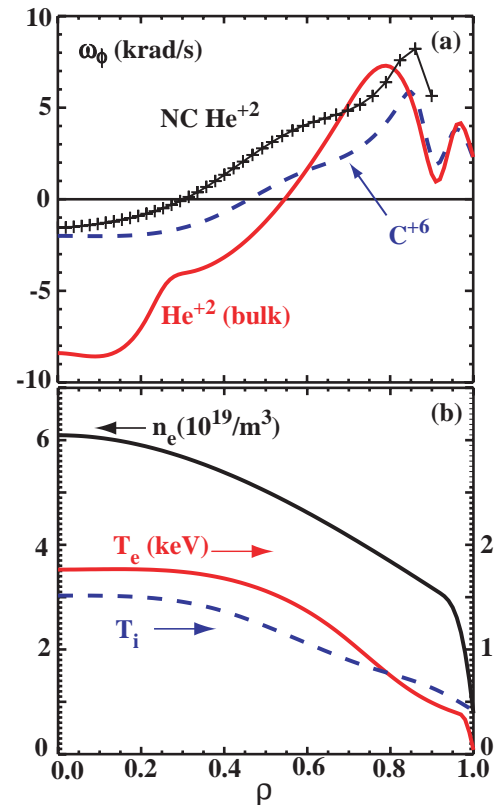


FIG. 7(a). Smooth fits to the measured rotation profiles for C and Helium in Helium discharges, and the neoclassical computation for He rotation based upon the other profile measurements. (b) Fits for the density and temperature profiles.